# First-principles study of magnetic interactions in 3*d* transition metal-doped phase-change materials

T. Fukushima* and H. Katayama-Yoshida
*Graduate School of Engineering Science, Osaka University, 1-3 Machikaneyama, Toyonaka, Osaka 560-8531, Japan*

K. Sato
*Graduate School of Engineering, Osaka University, 2-1 Yamadaoka, Suita, Osaka 565-0871, Japan*

H. Fujii
*Japan Synchrotron Radiation Research Institute, SPring-8, 1-1-1, Kouto, Sayo-cho, Sayo-gun, Hyogo 679-5198, Japan*

E. Rabel, R. Zeller, and P. H. Dederichs
*Peter Grünberg Institut and Institute for Advanced Simulation, Forschungszentrum Jülich and JARA, D-52425 Jülich, Germany*

W. Zhang and R. Mazzarello
*Institute for Theoretical Solid State Physics and JARA-Fundamentals of Future Information Technology, RWTH Aachen University, D-52056 Aachen, Germany*

(Received 19 August 2014; published 14 October 2014)

Recently, magnetic phase-change materials have been synthesized experimentally by doping with 3*d* transition metal impurities. Here, we investigate the electronic structure and the magnetic properties of the prototypical phase-change material $Ge_2Sb_2Te_5$ (GST) doped with V, Cr, Mn, and Fe by density functional calculations. Both the supercell method and the coherent potential approximation (CPA) are employed to describe this complex substitutionally disordered system. As regards the first approach, we consider a large unit cell containing 1000 sites to model the random distribution of the cations and of the impurities in doped cubic GST. Such a large-scale electronic structure calculation is performed using the program KKRnano, where the full potential screened Korringa-Kohn-Rostoker Green's function method is optimized by a massively parallel linear scaling (order-*N*) all-electron algorithm. Overall, the electronic structures and magnetic exchange coupling constants calculated by KKRnano agree quite well with the CPA results. We find that ferromagnetic states are favorable in the cases of V and Cr doping, due to the double exchange mechanism, whereas antiferromagnetic superexchange interactions appear to be dominant for Fe- and Mn-doped GST. The ferromagnetic interaction is particularly strong in the case of Cr. As a result, high Curie temperatures close to room temperatures are obtained for large Cr concentrations of 15%.

DOI: 10.1103/PhysRevB.90.144417 PACS number(s): 71.23.−k, 75.30.Hx

## I. INTRODUCTION

The development of novel device concepts to overcome the limitations of the Si-CMOS technology is a tremendous challenge. Nonvolatile memories based on phase-change materials (PCM) are a promising candidate, which offers high-density integration and high-speed read/write performance. For this reason, they have recently attracted a considerable amount of scientific and industrial interest [1]. Phase-change memories exploit the contrast in the electrical conduction properties of the amorphous (low-conductivity) and crystalline (high-conductivity) state of PCMs. Information stored in a memory cell is thus read out by measuring the electrical resistance. PCMs change rapidly and reversibly from the crystalline to the amorphous state at high temperature, which, in a memory cell, is induced by applying appropriate current pulses. Both phases are instead very stable at room temperature. Among the PCMs, the multicomponent chalcogenide $Ge_2Sb_2Te_5$ (GST) is the most widely used for data storage applications [2–5].

Recently, the possibility to add the spin degree of freedom to PCMs has been explored from the theoretical and experimental sides [6–10]. More specifically, Song *et al.* [6,7] obtained magnetic PCMs by incorporating Fe atoms into GST. They observed ferromagnetic behavior in both crystalline and amorphous phases by measuring the magnetic hysteresis curve, and estimated the Curie temperature ($T_C$) to be 173 K. They also showed that the two states exhibit a magnetic contrast, i.e., a different saturation magnetization. In principle, such a ferromagnetic PCM could open the way to realize a new multivalue memory, where the magnetic state as well as the electronic resistivity can be controlled by switching between the two phases. From the point of view of practical applications, the most crucial requirement is that the ferromagnetic $T_C$ is higher than room temperature. On the theoretical side, Li *et al.* [9] and Zhang *et al.* [10] performed density functional theory (DFT) [11,12] calculations and *ab initio* molecular dynamics simulations for crystalline and amorphous GST doped with several 3*d* transition metal (TM) impurities, including Cr, Mn, Fe, Co, and Ni. They focused on defect formation energies, electronic structures and magnitude of local magnetic moments in these systems. However, it has not yet been elucidated what the stable magnetic structures are, nor how they depend on the type of 3*d* dopant.

The purpose of this paper is to address this crucial issue. For this purpose, we study the electronic structure and the

*fuku@mp.es.osaka-u.ac.jp

 

magnetic properties of GST doped with V, Cr, Mn, and Fe. We determine the exchange mechanisms responsible for their magnetic order by calculating the exchange coupling constants ($J_{ij}$s) between the TM impurities. This enables us to determine the stable magnetic state for each of the four dopants. Moreover, we estimate $T_C$ for the systems showing ferromagnetic behavior by Monte Carlo simulations. We use the full potential Korringa-Kohn-Rostoker Green's function (KKR-GF) method [13,14], based on DFT. The KKR-GF method is an efficient tool for the study of magnetic systems and has been successfully applied to many TM-doped metals [15,16] and semiconductors [17]. In principle, the $J_{ij}$ coefficients can be evaluated by calculating the energy difference between ferromagnetic and antiferromagnetic spin configurations. However, arranging the magnetic moments of a dilute system in an antiferromagnetic fashion is not an easy task due to the sheer number of possible configurations. The KKR-GF method allows a direct calculation of the $J_{ij}$s from the scattering path operators by exploiting the magnetic force theorem, even for disordered systems. This approach is known as Lichtenstein's formula [18].

The outline of this paper is as follows. Section II describes the computational details and the models of TM-doped crystalline GST. In Sec. III, the calculated electronic structures, magnetic moments and $J_{ij}$s of V-, Cr-, Mn-, and Fe-doped GST are shown, and then the mechanisms stabilizing the ferromagnetic (antiferromagnetic) configuration in V- and Cr-doped GST (respectively, Mn- and Fe-doped GST) are discussed. Finally, our results are summarized in Sec. IV.

## II. COMPUTATIONAL METHODS

Previous studies have indicated that TM-doped GST is a substitutionally disordered system, where the TM impurities replace randomly the Ge or Sb atoms [8–10]. Interstitial and antisite configurations have higher formation energies and are not considered here. It is well known that electronic structure calculations of substitutionally disordered systems are not straightforward due to the absence of translational symmetry. Two computational schemes are often used to investigate their electronic structure. The first one is a mean-field approach called coherent potential approximation (CPA) [19,20]. In the CPA scheme, the multiple scattering effects occurring in a disordered system are replaced by scattering in an effective medium. The KKR-GF method is easily combined with CPA. However, CPA is a single-site approximation, which cannot describe short-range environmental effects of the individual configurations. Nonetheless, it is very popular due to its relatively low computational cost. The second approach is based on the use of supercells containing a large number of atoms, which are periodically repeated in space. The supercell method can describe disorder effects and local environment effects, however, very large cells are needed to include as many different configurations as possible and, at the same time, to avoid the artificial interactions originating from the periodicity. Here, we employ both methods and compare the results.

The stable crystalline phase of GST has hexagonal symmetry. However, it is known that, upon fast crystallization of amorphous GST, a metastable NaCl-type phase is formed,

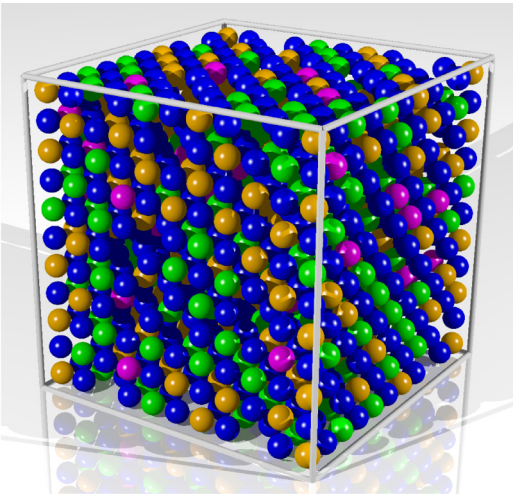

FIG. 1. (Color online) Structural model for the NaCl-type phase of $Ge_2Sb_2Te_5$ doped with TM impurities. Orange, green, magenta, and blue spheres indicate Ge, Sb, TM, and Te atoms, respectively.

wherein Ge, Sb, and vacancies ($V^c$) are randomly distributed into one face-centered cubic (fcc) sublattice, while Te atoms occupy the second one. In this work, we consider only the cubic phase, which is more relevant to applications. Therefore, we build a large "rocksalt" supercell and arrange Ge, Sb, TM atoms, and $V^c$s randomly in one sublattice (using a random number generator), as shown in Fig. 1. The supercell contains 1000 atoms, including 100 vacancies. More precisely, the stoichiometry is $Ge_{200-x}Sb_{200-y}TM_{x+y}V^c_{100}Te_{500}$, where $x+y$ is the number of TM impurities. We set $x+y=28$, corresponding to a TM concentration of about 3.1 %. Notice that, in the KKR method, the potentials of the $V^c$s are treated similarly as the atomic potentials. It is obviously computationally demanding to calculate such large magnetic systems by *ab initio* methods. Here we use the efficient KKRnano program package developed by Zeller *et al.* [21] and Thiess *et al.* [22,23]. KKRnano is based on the full-potential screened KKR method. The central part of this method is the solution of the Dyson equation for the Green's functions $G^{nn'}_{LL'}(E)$:

$$G^{nn'}_{LL'}(E) = G^{r,nn'}_{LL'}(E) + \sum_{n''L''L'''} G^{r,nn''}_{LL''}(E)\Delta t^{n''}_{L''L'''}(E)G^{n''n'}_{L'''L'}(E). \tag{1}$$

Here, $L=(l,m)$, where $l$ and $m$ are the angular momentum indices. $G^{nn'}_{LL'}(E)$ and $G^{r,nn'}_{LL'}(E)$ are the Green's function elements of the system under study and of a suitable reference system, respectively. $\Delta t^{n}_{LL'}(E) = t^{n}_{LL'}(E) - t^{r,n}_{LL'}(E)$ is the difference between the single site scattering $t$ matrices of the atoms in the true and reference system. In the screened KKR method, a system with strongly repulsive potentials is used as a reference system [21], such that the Green's functions $G^{r,nn'}_{LL'}(E)$ decrease very rapidly at large distances ($|\boldsymbol{R}^n - \boldsymbol{R}^{n'}|$). Contrary to the standard KKR-GF method, KKRnano allows order-$N$ scaling of the computational cost by truncating the Green's function and solving the Dyson equation iteratively, based on the quasi minimal residual method with block-circulant matrix

preconditioning [24,25]. Since the charge density and density of states are directly related to the imaginary part of the Green's function, one can use the KKR-GF method in the framework of density functional theory. For the exchange correlation functional, we employ the local density approximation (LDA) in the form proposed by von Barth and Hedin [26], with the parameters determined by Moruzzi *et al.* [27]. We perform MPI/OpenMP hybrid parallel calculations using 12 000 processes on the IBM Blue Gene/Q (JUQUEEN) computer in the Jülich Supercomputing Center [28].

To investigate the magnetic interaction between the TM impurities, we calculate $J_{ij}$ by Lichtenstein's formula [18], which avoids the calculation of the total energy difference between ferromagnetic and antiferromagnetic states. In this approach, the classical Heisenberg model is assumed and $J_{ij}$s are obtained from

$$J_{ij} = \frac{1}{4\pi}\mathrm{Im}\int^{E_F} dE\ \mathrm{Tr}_L\{\Delta_i T_\uparrow^{ij}\Delta_j T_\downarrow^{ij}\}, \qquad (2)$$

where $\Delta_i = t_{i\uparrow}^{-1} - t_{i\downarrow}^{-1}$, with $t_{i\uparrow(\downarrow)}$ being the atomic $t$-matrix of the TM impurity at site $i$ for the spin up (down) state. $T_{\uparrow(\downarrow)}^{ij}$ is the scattering path operator between site $i$ and $j$ for the spin up (down) state. $\mathrm{Tr}_L$ is the trace over the orbital variables. Then, $T_C$ of magnetic GST is estimated by using the calculated $J_{ij}$s and Monte Carlo simulations together with Binder's cumulant method [29].

In the present calculations, the lattice constant is fixed to the experimental value [30]: $a = 11.393\ a_B$, where $a_B$ is the Bohr radius. The maximum angular momentum in the expansion of the wave functions and Green's function is set to $l_{max} = 2$. Our calculations are performed with single Γ-point $k$-space sampling. Ge $4s4p$, Sb $5s5p$, Te $5s5p$, and TM $4s3d$ electrons are treated as valence electrons. In our KKRnano simulations, we do not relax the atomic positions. Relaxation effects are small in the case of V, Cr, and Mn [10] but can be significant for Fe-doped GST [8]. This point is further discussed at the end of section III B.

## III. RESULTS

### A. Electronic structure

Local density of states (LDOSs) of (a) Ge, (b) $V^c$, (c) Sb, and (d) Te for all the individual sites in the Cr-doped cubic GST system calculated by KKRnano are shown in Fig. 2. The Ge-4$s$ and Sb-5$s$ states mostly lie from −10 to −6 eV, the Te-5$s$ states are mainly located between −14 and −10 eV, and the Te-5$p$ states make the largest contribution to the valence band. The thick lines in Fig. 2, which correspond to the averaged LDOSs over the individual sites, are in good agreement with the previous works by Caravati *et al.* [31]. Figure 3 shows the LDOSs for the majority and minority spin states of TM doped cubic GST, calculated by KKRnano. Plots (a), (b), (c), and (d) are the 3$d$ LDOSs of all the individual V, Cr, Mn and Fe atoms, respectively.

For each type of TM atom, the 3$d$ LDOSs depend on the local environment of the individual sites: although each TM impurity has six nearest-neighbor Te atoms, Ge, Sb, TM atoms and $V^c$ occupy randomly the second nearest-neighbor sites. The LDOSs of all the TM impurities have sharp virtual

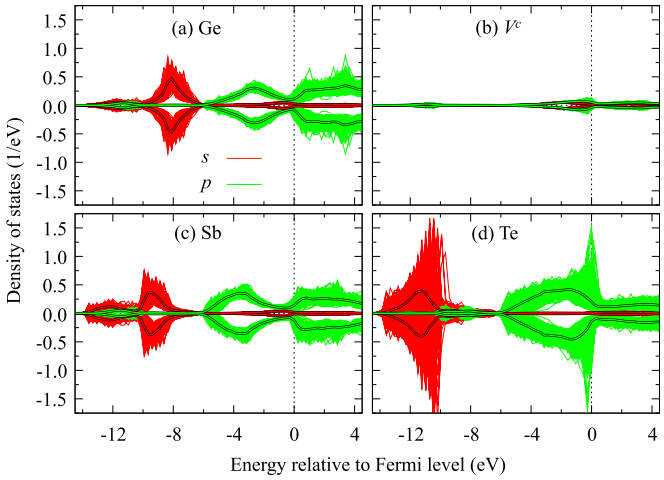


FIG. 2. (Color online) Local density of states (LDOSs) of (a) Ge, (b) $V^c$, (c) Sb and (d) Te in Cr-doped cubic GST calculated by KKRnano. The LDOSs for majority and minority spin states on all the individual sites are shown. The averaged LDOSs over the individual sites are indicated by the thick lines in the corresponding colors.

bound states with an exchange splitting leading to a finite local magnetic moment. The sharp peaks in the majority spin states move to lower energies in the sequence from V to Mn dopants. The largest exchange splitting (∼3.91 eV) is realized in the Mn doped case. In V-, Cr-, and Fe-doped GSTs, the states at the Fermi level ($E_F$) have predominantly TM-3$d$ character and the contribution from the other orbitals is very small. This fact will become important when discussing the stable magnetic state (see Sec. III B). Our LDOSs for Cr, Mn, and Fe atoms calculated using KKRnano are consistent with previous results obtained by a plane wave code based on the pseudo potential method [9,10]. To the best of our knowledge, doping of GST by V has not been investigated before.

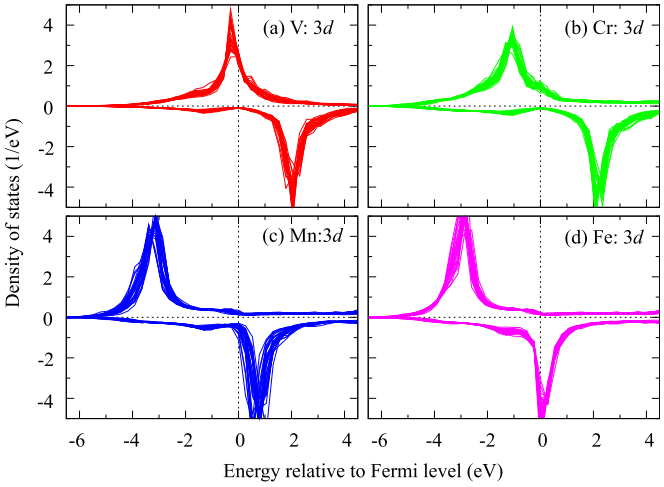


FIG. 3. (Color online) 3$d$ local density of states (LDOSs) of (a) V-, (b) Cr-, (c) Mn-, and (d) Fe-doped cubic GST calculated by KKRnano. The LDOSs for majority and minority spin states on all the individual TM sites are shown. The concentration of the TM impurities is 3.1%.

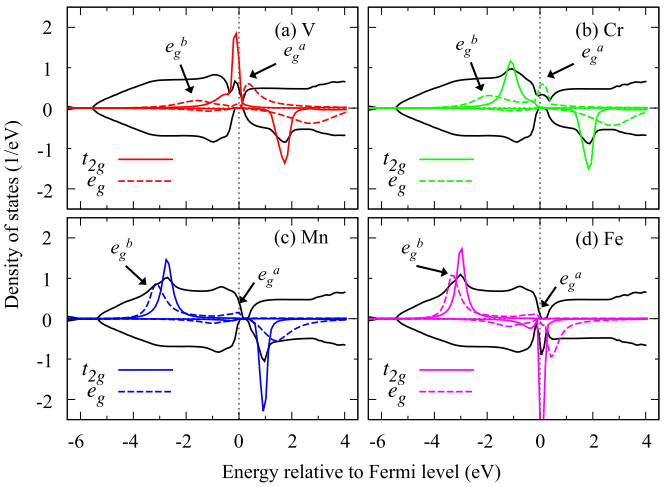


FIG. 4. (Color online) 3*d* LDOSs of (a) V-, (b) Cr-, (c) Mn-, and (d) Fe-doped cubic GST calculated by CPA. The TM impurity concentration is 3.1% for all the models. The solid and dashed lines indicate the $t_{2g}$ and $e_g$ components, respectively. The bonding ($e_g^b$) and antibonding ($e_g^a$) states are indicated by black arrows. The total density of states are also shown by the black lines.

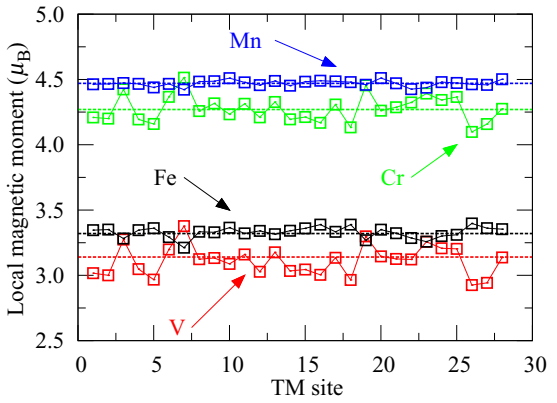


FIG. 5. (Color online) Local magnetic moments of the 28 individual TM impurities within the Wigner-Seitz spheres in V-, Cr-, Mn-, and Fe-doped cubic GST. The local moments are obtained from the KKRnano simulations by integrating within the Wigner-Seitz spheres. The magnetic moments averaged over the individual sites are indicated by the dashed lines.

The ligand field theory is useful to roughly understand the electronic structure of magnetic GST. Due to the crystal field for the octahedral, $O_h$, symmetry of the NaCl type structure, the TM-3*d* states split into $e_g$ ($x^2-y^2$, $3z^2-r^2$) and $t_{2g}$ ($xy$, $yz$, $zx$) states. The $t_{2g}$ states have nonbonding character because they extend into the interstitial region. In particular, the hybridization between the TM-$t_{2g}$ and the Te-5*p* states is weak. Hence these states correspond to sharp peaks in the LDOSs. On the other hand, the impurity $e_g$ states hybridize strongly with the Te-5*p* states, leading to well-separated bonding ($e_g^b$) and antibonding ($e_g^a$) states.

These bonding mechanisms are reproduced by our CPA calculations. Figure 4 shows the TM-3*d* LDOSs decomposed into the $e_g$ and $t_{2g}$ states obtained by CPA. The black arrows in Fig. 4 indicate the positions of the bonding $e_g^b$ and antibonding $e_g^a$ states. These states correspond to a broad and a rather narrow peak, respectively. In the V doped case, $E_F$ crosses the majority-spin $t_{2g}$ states but there are also small contributions from the $e_g^a$ states at $E_F$. When the dopant is Cr, the $t_{2g}$ states are fully occupied and the states at $E_F$ have mainly $e_g^a$ character. Therefore, half-metallic ground states are obtained in the V and Cr cases. For Mn dopants, all the majority spin 3*d* states are occupied. On the other hand, for Fe atoms, the minority spin states begin to be occupied. As a result, the nonbonding minority-spin $t_{2g}$ states are predominant at $E_F$. For a given TM impurity, the electronic structure of doped GST is very similar to that of the corresponding doped parent compound GeTe [32–34]. It is important to mention that our models of GST exhibit a pseudo band gap, whereas, experimentally, the gap of cubic GST is of order 0.5 eV [35]. The discrepancy is due to the use of approximate LDA functionals and can be partially cured by employing GGA and hybrid functionals, which yield band gap values of 0.37 and 0.6 eV, respectively, as reported in the work by Caravati *et al.* [31].

### B. Magnetic properties

#### 1. *Local magnetic moments*

Figure 5 shows the local magnetic moments of the TM impurities in cubic GST, obtained from the KKRnano simulations by integrating within the Wigner-Seitz spheres. The whole crystal is partitioned into Wigner-Seitz cells by the Voronoi construction. The radii of all the Wigner-Seitz spheres are the same in the crystalline phase, therefore the deviations in the local magnetic moment of the individual TM impurities reflect the local environment of the ligand atoms. We also calculated the local moments within CPA, using the MACHIKANEYAMA code [36]. The magnetic moments averaged over all the impurities of a given type are 3.14 (2.85), 4.27 (3.93), 4.47 (4.31), and 3.32 (3.30) $\mu_B$ for V, Cr, Mn, and Fe atoms, respectively, where the values in brackets refer to the CPA results. The KKR-CPA code uses spherical muffin-tin potentials and the integration volume for the local moments is the muffin-tin sphere, whereas KKRnano is a full potential code and the integration volume for the local moments is the Voronoi cell, as already mentioned. For this reason, the local moments obtained by KKRnano are larger, since the cell volume is considerably larger than the muffin-tin volume. This is particularly important for the V and Cr moments, since their 3*d* orbitals are more extended. Nevertheless, the qualitative trends in magnitude are the same. As shown in Figs. 3 and 4, the majority spin states are gradually occupied while moving from V to M, resulting in the increase of the local magnetic moments. In fact, if one assumes that the Ge and Sb cations are in 2+ and 3+ valence states, respectively, the Mn atoms (which have $3d^5 4s^2$ configuration in the atomic state) should display the maximum magnetic moment value of 5 at the Ge site.

#### 2. *Exchange coupling constants* $J_{ij}$

One can estimate the magnetic interaction between the TM impurities quantitatively from the calculation of the $J_{ij}$ constants by the Lichtenstein's formula, Eq. (2). As

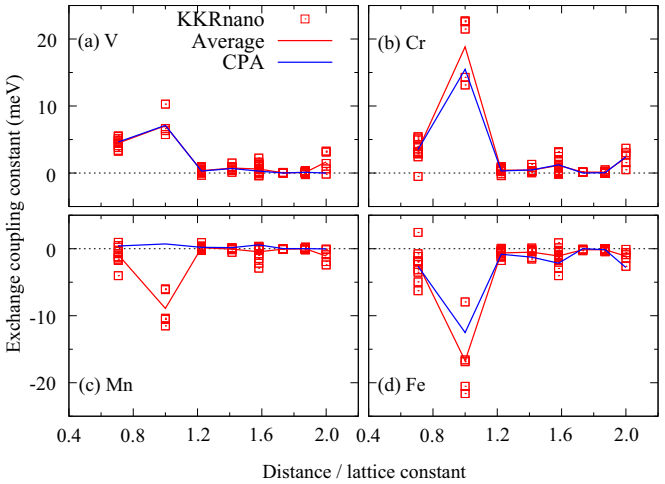


FIG. 6. (Color online) Exchange coupling constants ($J_{ij}$s) as a function of the distance between two TM impurities in (a) V, (b) Cr, (c) Mn, and (d) Fe 3.1% doped cubic GST, calculated by KKRnano (red squares) and CPA (blue lines). The KKRnano values of $J_{ij}$ calculated by averaging over all the pairs at a given distance are also shown by the red lines. A positive (negative) value means ferromagnetic (antiferromagnetic) interaction.

discussed in Sec. II, our 1000-site supercell contains 28 TM atoms. The random number generator used to generate the structure yields a configuration containing 11 TM dimers on first nearest-neighbor fcc sites and five TM dimers on second nearest-neighbor sites. Due to the NaCl structure and the resulting pronounced hybridization of the $e_g$ impurity states with the Te-5$p$ states, one expects strong second nearest-neighbor interactions and relatively weak first nearest-neighbor interactions. The latter ones basically arise from the interaction of the nonbonding $t_{2g}$ states. The calculated $J_{ij}$s for (a) V, (b) Cr, (c) Mn, and (d) Fe atoms in the 3.1% doped GST as a function of the distance between the TM impurities are shown in Fig. 6. The red squares and blue lines are the KKRnano and CPA results, respectively. The red lines are the KKRnano values averaged over the impurities. At a given distance, the $J_{ij}$ values obtained by KKRnano are widely fluctuating. This stems from the fact that local environment effects strongly affect the magnetic interactions. Such behavior is most severe for the second nearest-neighbor interactions which, depending on the environment, can vary by a factor of 2. Nevertheless, upon averaging over the different configurations, the KKRnano results are consistent with the CPA results (except for the Mn case, which is discussed below). This shows that the randomness in the TM impurity distribution is reasonably well described by the large supercells used in our KKRnano calculations. On the other hand, it also shows that the environment-induced fluctuations are quite large and cannot be described by a mean-field approach like CPA.

The V- and Cr-doped GST exhibit positive $J_{ij}$s, leading to ferromagnetic interactions between the TM impurities. In particular, for the Cr doped case, very large ferromagnetic interactions are realized at the second nearest neighbors, corresponding to 180° TM-Te-TM bondings. An echo of this strong bonding is seen for the 8th nearest neighbors at (2,0,0) positions, which always display the same type of interaction as the second nearest neighbors (on (1,0,0) sites). If doping of GST at Cr concentrations higher than the magnetic percolation threshold is possible, one can expect high-$T_C$ values in this system. Although there is no experimental data for Cr-doped GST, Song *et al.* have reported that, in the case of Fe doped GST, a high doping concentration of up to 19% is possible, without any precipitation. Therefore we have performed calculations of $T_C$ for the Cr 10% and 15% doped systems. In the mean-field approximation, we obtain $T_C$ values of about 298 and 275 K for the 10% and 15% Cr concentrations, respectively. However, it is well known that the mean field approximation overestimates $T_C$ for dilute systems [17]. An accurate calculation by Monte Carlo simulations using Binder's cumulant treatment [29] yields 207 and 239 K for the 10% and 15% Cr-doped GST. Even higher Cr concentrations may be experimentally attainable, resulting in $T_C$ values comparable to room temperature.

For Fe-doped GST, it is worthwhile to compare our results with previous experimental and theoretical works [6–8]. Ferromagnetism has been observed in experiments, whereas both KKRnano and CPA calculations indicate that the antiferromagnetic state is stable. The fact that we focused on the cubic phase, whereas in said previous works the hexagonal phase was investigated, cannot account for such discrepancy, in that, according to Ref. [9], the electronic structures of Fe-doped cubic and hexagonal GST are very similar. Here, it is important to stress again that we did not relax our models. Relaxation effects are small in the case of Cr and Mn [10], however, both low- [8,10] and high-spin [9,10] configurations have been shown to exist in Fe-doped GST. The former states are characterized by short Fe-Te bond lengths (hence, large relaxation) and strong crystal-field effects, whereas the latter exhibit long Fe-Te bonds. In the calculations performed in this paper, only high spin configurations are found for substitutional TM impurities on Ge and Sb sites. Although DFT calculations show that the low spin states are less stable than the high-spin ones [10], the former yield saturation magnetizations in better agreement with experimental data. Furthermore, calculations of energy differences between ferromagnetic and antiferromagnetic configurations [8] indicate that, in the low-spin case, for some distances and arrangements of the pairs of Fe impurities, the coupling may indeed be ferromagnetic. Another important ingredient may turn out to be the presence of excess Ge and/or Sb vacancies, which are known to be responsible for the large concentrations of hole carriers in crystalline GST [31]. These two points need further investigation.

### 3. *Origin of ferromagnetic and antiferromagnetic couplings*

Next, we consider the origin of ferromagnetism and antiferromgnetism in TM-doped GST. Belhadji *et al.* [17,37] proposed a set of rules for understanding qualitatively the trends in exchange interactions and the stability of different magnetic configurations in DMSs, based on the inspection of the electronic structure. According to these rules, the magnetic structure of DMSs is determined by the interplay between three exchange mechanisms, namely double exchange, kinetic $p$-$d$ exchange and superexchange. The first two mechanisms

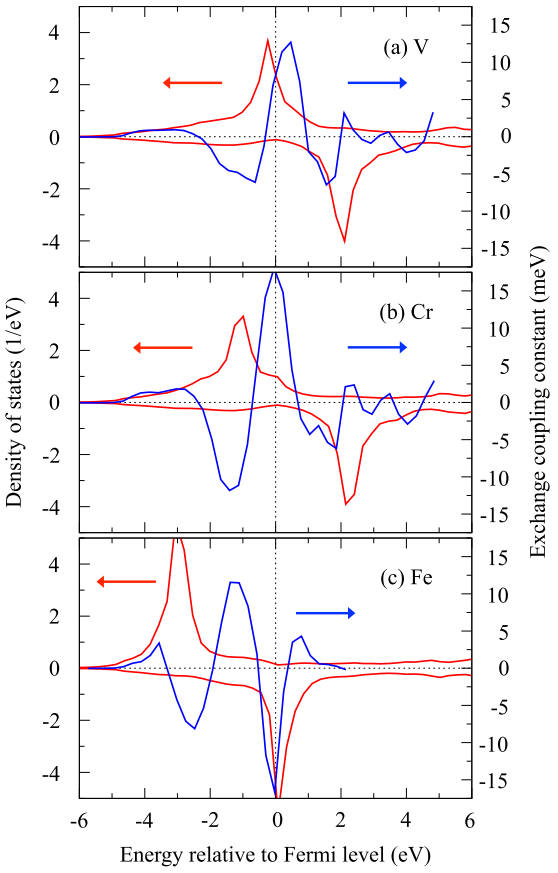


FIG. 7. (Color online) Configuration averaged exchange coupling constant $J_{ij}(E)$ between second nearest-neighbor TM impurities (blue line, right scale) and 3*d* LDOSs (red line, left scale) as a function of energy for (a) V-, (b) Cr-, and (c) Fe-doped GST calculated by KKRnano.

favor ferromagnetism and require a finite density of states at $E_F$, namely TM-*d* states (double-exchange) or anion *p* states (*p*-*d* exchange). Superexchange typically leads to antiferromagnetism but can also favor ferromagnetism [e.g., in (Ga,V)As]. This mechanism can be effective in the absence of carriers as well. We apply these rules to TM-doped GST.

First we discuss the exchange interactions for V, Cr, and Fe impurities in GST. In Fig. 7, we show the averaged LDOSs for V, Cr, and Fe impurities (red curve, left vertical axis), as calculated by KKRnano. We also show the (artificial) exchange coupling constants $J_{ij}(E)$s obtained from Eq. (2) by replacing the Fermi level $E_F$ with a variable energy $E$ (blue curve, right vertical axis). These plots indicate that, in the case of Cr, $J_{ij}(E)$ reaches its maximum value at $E_F$, showing that Cr impurities are the ideal choice for robust ferromagnetism. Physically, the energy gain for ferromagnetic coupling arises from the double exchange mechanism: more specifically, the reduction in energy is due to the hybridization and the consequent broadening of the $e_g^{a\uparrow}$ states (located at $E_F$) of pairs of Cr impurities on the second nearest-neighbor sites. For the V impurity case, the $J_{ij}(E)$ value is smaller at $E_F$ compared to the Cr case. This is because the main component at $E_F$ is the $t_{2g}^{\uparrow}$ states and the contribution from the $e_g^{a\uparrow}$ states is rather small, which results in the weaker ferromagnetic

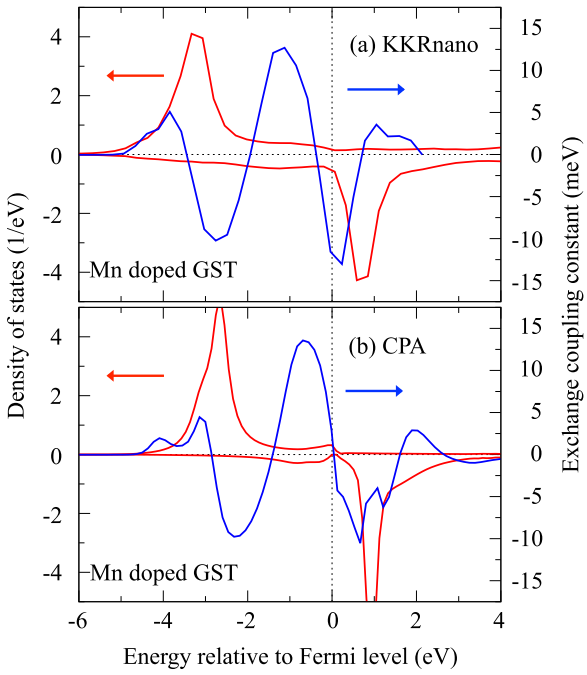


FIG. 8. (Color online) Configuration averaged exchange coupling constant $J_{ij}(E)$ between second nearest-neighbor Mn impurities (blue line, right scale) and 3*d* LDOSs (red line, left scale) as a function of energy for Mn-doped GST calculated by (a) KKRnano and (b) CPA.

interaction. In the case of Fe impurities, the situation is very different. Here, the $e_g^{a\uparrow}$ and $e_g^{a\downarrow}$ states are slightly below and above $E_F$, respectively. Hence strongly interacting pairs of Fe impurities at the second nearest-neighbor sites prefer to have opposite magnetic moments, so that the empty upper $e_g^a$ peak of one impurity hybridizes with the occupied lower $e_g^a$ peak of the second one. An antiferromagnetic coupling stabilized by the superexchange mechanism is thus observed. Interestingly, for energies slightly below $E_F$, the $J_{ij}(E)$ curve for Fe rapidly changes from negative to positive values. Around $-1$ eV, this curve resembles the one for Cr near $E_F$. The behavior for Mn is expected to be intermediate with respect to Cr and Fe. Hence the predominant magnetic coupling in Mn-doped GST should be very sensitive to the exact position of $E_F$. This fact is clearly seen in Fig. 8, where the results of the averaged 3*d* LDOSs and $J_{ij}(E)$ for Mn-doped GST calculated by KKRnano and CPA are compared. The $J_{ij}(E)$ values for Mn calculated by CPA are nearly zero, whereas the more accurate KKRnano values indicate (relatively weak) antiferromagnetic coupling. Note that the KKRnano calculations yield considerably broader $t_{2g}$ and $e_g$ peaks of the TM impurities than the CPA, which we attribute to higher order scattering effects neglected in the CPA. A comparison of Fig. 3 and 4 clearly shows the stronger broadening in the KKRnano case.

## IV. SUMMARY

In this work, we have presented first-principles investigations of the electronic structure and the magnetic properties of TM-doped crystalline GST. We have determined the local density of states, local magnetic moments and exchange

coupling constants $J_{ij}$s of V-, Cr-, Mn-, and Fe-doped GST, by means of the KKR-GF method. We have considered both the supercell method (using a large unit cell containing 1000 atoms) and the CPA scheme. The KKRnano program, which allows massively parallel linear scaling calculations, has been employed for the supercell calculations. The different local atomic environments observed in the supercell calculations lead to large fluctuations in the $J_{ij}$ values, which cannot be described by CPA. Nevertheless, the averaged $J_{ij}$ values obtained from the KKRnano calculations agree well with the CPA results, except for the Mn doped case. We have shown that the ferromagnetic ordering is stable for V- and Cr-doped GST, while the antiferromagnetic interaction is dominant for Mn- and Fe-doped systems. Experimentally, Fe-doped GST appears to be ferromagnetic. The discrepancy may be due to the existence of metastable low spin configurations, predicted by previous DFT calculations, which have not been considered in this work. This point requires further investigation. Cr-doped GST is particularly interesting, in that it exhibits strong ferromagnetic interactions. The ferromagnetic state is stabilized by the double exchange coupling originating from the Cr anti-bonding $e_g^{a\uparrow}$ states, which lie at $E_F$. The Curie temperature of this system, estimated by Monte Carlo simulations in combination with the Binder's cumulant method, turns out to be 207 K (respectively, 239 K) for 10% (respectively 15%) Cr concentration. Although these temperature values are still too low for real applications, it may be possible to increase them up to room temperature by further increasing the concentration of impurities or by changing the stoichiometry of the host material.

## ACKNOWLEDGMENTS

The authors acknowledge the financial support from JSPS Core-to-Core Program, A. Advanced Research Networks. K.S. thanks Grant-in-Aid for Scientific Research on Innovative Areas "Materials Design through Computics: Complex Correlation and Non-Equilibrium Dynamics." W.Z. and R.M. acknowledge funding by the DFG (German Science Foundation) within the collaborative research center SFB 917 "Nanoswitches." Computational time provided by the Jülich Supercomputing Centre is also acknowledged. The plot of the crystal structure in Fig. 1 was prepared using the software POV-Ray.

[1] M. Wuttig and N. Yamada, Nat. Mater. **6**, 824 (2007).
[2] A. V. Kolobov, P. Fons, A. I. Frenkel, A. L. Ankudinov, J. Tominaga, and T. Uruga, Nat. Mater. **3**, 703 (2004).
[3] D. Lencer, M. Salinga, B. Grabowski, T. Hickel, J. Neugebauer, and M. Wuttig, Nat. Mater. **7**, 972 (2008).
[4] W. Welnic, A. Pamungkas, R. Detemple, C. Steimer, S. Blügel, and M. Wuttig, Nat. Mater. **5**, 56 (2006).
[5] Z. Sun, J. Zhou, and R. Ahuja, Phys. Rev. Lett. **96**, 055507 (2006).
[6] W.-D. Song, L.-P. Shi, X.-S. Miao, and T.-C. Chong, Adv. Mater. **20**, 2394 (2008).
[7] W.-D. Song, L.-P. Shi, and T.-C. Chong, J. Nano. Nanotechnol. **11**, 2648 (2011).
[8] D. Ding, K. Bai, W. D. Song, L. P. Shi, R. Zhao, R. Ji, M. Sullivan, and P. Wu, Phys. Rev. B **84**, 214416 (2011).
[9] Y. Li and R. Mazzarello, Adv. Mater. **24**, 1429 (2012).
[10] W. Zhang, I. Ronneberger, Y. Li, and R. Mazzarello, Adv. Mater. **24**, 4387 (2012).
[11] P. Hohenberg and W. Kohn, Phys. Rev. **136**, B864 (1964).
[12] W. Kohn and L. J. Sham, Phys. Rev. **140**, A1133 (1965).
[13] J. Korringa, Physica **13**, 392 (1947).
[14] W. Kohn and N. Rostoker, Phy. Rev. **94**, 1111 (1954).
[15] R. Podloucky, R. Zeller, and P. H. Dederichs, Phys. Rev. B **22**, 5777 (1980).
[16] R. Zeller and P. H. Dederichs, Phys. Rev. Lett. **42**, 1713 (1979).
[17] K. Sato, L. Bergqvist, J. Kudrnovský, P. H. Dederichs, O. Eriksson, I. Turek, B. Sanyal, G. Bouzerar, H. Katayama-Yoshida, V. A. Dinh, T. Fukushima, H. Kizaki, and R. Zeller, Rev. Mod. Phys. **82**, 1633 (2010).
[18] A. I. Liechtenstein, M. I. Katsnelson, V. P. Antropov, and V. A. Gubanov, J. Magn. Magn. Mater **67**, 65 (1987).
[19] P. Soven, Phys. Rev. B **2**, 4715 (1970).
[20] H. Shiba, Prog. Theor. Phys. **46**, 77 (1971).
[21] R. Zeller, J. Phys.: Condens. Matter **20**, 294215 (2008).
[22] A. Thiess, R. Zeller, M. Bolten, P. H. Dederichs, and S. Blügel, Phys. Rev. B **85**, 235103 (2012).
[23] A. Thiess, Ph.D. thesis, RWTH Aachen, 2011.
[24] R. W. Freund and N. M. Nachtigal, Num. Math **60**, 315 (1991).
[25] M. Bolten, A. Thiess, I. Yavneh, and R. Zeller, Linear Algebra Appl. **436**, 436 (2012).
[26] U. von Barth and L. Hedin, J. Phys. C: Solid State Phys. **5**, 1629 (1972).
[27] V. L. Moruzzi, J. F. Janak, and A. R. Williams, Phys. Rev. B **12**, 1257 (1975).
[28] http://www.fz-juelich.de/ias/jsc/juqueen.
[29] K. Binder and D. W. Heermann, *Monte Carlo Simulation in Statistical Physics* (Springer, Berlin, 2002).
[30] T. Nonaka, G. Ohbayashi, Y. Toriumi, Y. Mori, and H. Hashimoto, Thin Solid Films **370**, 258 (2000).
[31] S. Caravati, M. Bernasconi, T. D. Kühne, M. Krack, and M. Parrinello, J. Phys.: Condens. Matter **21**, 255501 (2009).
[32] K. Sato and H. Katayama-Yoshida, J. Non-Cryst. Solids **358**, 2377 (2012).
[33] Y. Liu, S. K. Bose, and J. Kudrnovský, J. Appl. Phys. **112**, 053902 (2012).
[34] W. Zhang, I. Ronneberger, Y. Li, and R. Mazzarello, Sci. Adv. Mater. **6**, 1655 (2014).
[35] B.-S. Lee, J. R. Abelson, S. G. Bishop, D.-H. Kang, B.-K. Cheong, and K.-B. Kim, J. Appl. Phys. **97**, 093509 (2005).
[36] H. Akai, J. Phys. Soc. Jpn. **51**, 468 (1982).
[37] B. Belhadji, L. Bergqvist, R. Zeller, P. H. Dederichs, K. Sato, and H. Katayama-Yoshida, J. Phys.: Condens. Matter **19**, 436227 (2007).